



UNIVERSITY OF LEEDS

This is a repository copy of *Evaluating morphological estimates of the aerodynamic roughness of debris covered glacier ice*.

White Rose Research Online URL for this paper:  
<http://eprints.whiterose.ac.uk/118630/>

Version: Accepted Version

---

**Article:**

Quincey, DJ, Smith, MW [orcid.org/0000-0003-4361-9527](https://orcid.org/0000-0003-4361-9527), Rounce, DR et al. (3 more authors) (2017) Evaluating morphological estimates of the aerodynamic roughness of debris covered glacier ice. *Earth Surface Processes and Landforms*, 42 (15). pp. 2541-2553. ISSN 0197-9337

<https://doi.org/10.1002/esp.4198>

---

This article is protected by copyright. All rights reserved. This is the peer reviewed version of the following article: Quincey, D. J., Smith, M. W., Rounce, D. R., Ross, A. N., King, O., and Watson, C. S. (2017) Evaluating morphological estimates of the aerodynamic roughness of debris covered glacier ice. *Earth Surf. Process. Landforms*, which will be published in final form at <https://doi.org/10.1002/esp.4198>. This article may be used for non-commercial purposes in accordance with Wiley Terms and Conditions for Self-Archiving.

**Reuse**

Items deposited in White Rose Research Online are protected by copyright, with all rights reserved unless indicated otherwise. They may be downloaded and/or printed for private study, or other acts as permitted by national copyright laws. The publisher or other rights holders may allow further reproduction and re-use of the full text version. This is indicated by the licence information on the White Rose Research Online record for the item.

**Takedown**

If you consider content in White Rose Research Online to be in breach of UK law, please notify us by emailing [eprints@whiterose.ac.uk](mailto:eprints@whiterose.ac.uk) including the URL of the record and the reason for the withdrawal request.



[eprints@whiterose.ac.uk](mailto:eprints@whiterose.ac.uk)  
<https://eprints.whiterose.ac.uk/>

# Evaluating morphological estimates of the aerodynamic roughness of debris covered glacier ice

Quincey, D.J.<sup>1,\*</sup>, Smith, M.W.<sup>1</sup>, Rounce, D.R.<sup>2</sup>, Ross, A.N.<sup>3</sup>, King, O.<sup>1</sup> and Watson, C.S.<sup>1</sup>

1. School of Geography, University of Leeds, LS2 9JT, UK

2. Center for Research in Water Resources, University of Texas at Austin, Austin, Texas, USA

3. School of Earth and Environment, University of Leeds, LS2 9JT, UK

\* correspondence to [d.j.quincey@leeds.ac.uk](mailto:d.j.quincey@leeds.ac.uk)

## Abstract

Aerodynamic roughness length ( $z_0$ ), the height above the ground surface at which the extrapolated horizontal wind velocity profile drops to zero, is one of the most poorly parameterised elements of the glacier surface energy balance equation. Microtopographic methods for estimating  $z_0$  have become prominent in the literature in recent years, but are rarely validated against independent measures and are yet to be comprehensively analysed for scale or data resolution dependency. Here, we present the results of a field investigation conducted on the debris covered Khumbu Glacier during the post-monsoon season of 2015. We focus on two sites. The first is characterised by gravels and cobbles supported by a fine sandy matrix. The second comprises cobbles and boulders separated by voids. Vertical profiles of wind speed recorded by a tower comprising five cup anemometers and deployed over both sites enable us to derive measurements of aerodynamic roughness that reflect their

This article has been accepted for publication and undergone full peer review but has not been through the copyediting, typesetting, pagination and proofreading process which may lead to differences between this version and the Version of Record. Please cite this article as doi: 10.1002/esp.4198

observed surface characteristics (0.0184 m and 0.0243 m respectively). At the second site,  $z_0$  also varied through time following snowfall (0.0055 m) and during its subsequent melt (0.0129 m), showing the importance of fine resolution topography for near-surface airflow. To compare the wind profile data to microtopographic methods, we conducted Structure from Motion Multi-View Stereo (SfM-MVS) surveys across each patch and calculated  $z_0$  using three previously published approaches. The fully three-dimensional cloud-based approach is shown to be most stable across different scales and these  $z_0$  values are most correct in relative order when compared to the wind tower data. Popular profile-based methods perform less well providing highly variable values across different scales and when using data of differing resolution. These findings hold relevance for all studies using microtopographic methods to estimate aerodynamic roughness lengths, including those in non-glacial settings.

Keywords: debris-covered ice; roughness; Structure from Motion; Himalaya; microtopography.

## 1. Introduction

Debris-covered ice is present in all glacierised regions of the world (Scherler et al., 2011; Röhl, 2008; Racoviteanu et al., 2008) and is known to respond to climatic variability non-linearly because of the insulating effect of the surface layer (Benn et al., 2012; Nicholson and Benn 2006). As well as promoting a complex surface topography and a suite of mass loss processes not commonly found on debris-free glaciers (Thompson et al., 2016), the presence of a debris layer directly affects rates of melt, either by enhancing or restricting heat transfer to the ice surface (Østrem, 1959; Nicholson and Benn, 2006). The turbulent fluxes of sensible and latent heat

play an important role in completing the surface energy budget (Hock, 2005), but are particularly difficult to represent in modelling studies because of a lack of empirical data describing key surface processes and characteristics.

Aerodynamic roughness length ( $z_0$ ), the length scale that characterises loss of wind momentum attributable to surface roughness (Chappell and Heritage, 2007), remains a major uncertainty when determining turbulent heat fluxes over all glacier surfaces, and can vary by an order of magnitude even within a small area and over the ablation season (Smeets et al., 1999; Arnold and Rees, 2003). Its correct parameterisation is critical in surface energy balance studies, since an order of magnitude change in  $z_0$  can lead to a factor of 2 change in estimated turbulent fluxes (Munro, 1989; Hock and Holgrem, 1996; Brock et al., 2006). An increasing number of studies have sought to develop methods for quantifying  $z_0$  over glacierised (e.g. Irvine-Fynn et al., 2014; Smith et al., 2016) and non-glacierised surfaces (e.g. Eitel et al., 2011; Smith et al., 2011) and have shown that digital elevation data derived from photogrammetry and terrestrial laser scanning can provide estimates of surface roughness where independent aerodynamic measurements are not available (Nield et al., 2012). Such proxies are attractive because they may alleviate the need to construct and maintain cumbersome meteorological stations on often difficult-to-access glacier surfaces. Nonetheless, quantifying both spatial variation and temporal change of  $z_0$  remains a key research challenge.

Defining  $z_0$  over debris-covered ice is particularly complex, because the surface may comprise clasts of greatly varying size, and the broader-scale surface relief can be similarly heterogeneous. Most modelling studies to date have assumed a single  $z_0$  value to represent the whole glacier surface (e.g. Foster et al., 2012) but the ability to data model debris-covered surfaces at the centimetric scale opens up the possibility

of calculating spatially- and temporally-varying  $z_0$  based on measurements of surface microtopography (Rounce et al., 2015). However, few have validated these assumed or measured values of  $z_0$  with independent vertical wind profile measurements (Brock et al., 2006), or considered how the measurements vary over a range of different surface types or scales of analysis. This holds true for studies focussing on debris-free as well as debris-covered glacier ice (Smith et al., 2016; Rounce et al., 2015), and is a critical step if robust relationships between surface roughness and backscatter signals from airborne or satellite platforms are ever to be realised (e.g. Blumberg and Greeley, 1993; Rees and Arnold, 2006).

Using microtopographic and aerodynamic measurements of  $z_0$  over the debris-covered Khumbu Glacier, Nepal, we aimed to evaluate the validity of the morphological approach. We set out to answer four research questions:

1. How dependent are microtopographic estimations of  $z_0$  on the method used?
2. How dependent are microtopographic estimations of  $z_0$  on the area of the plot used in the analysis?
3. How dependent are microtopographic estimations of  $z_0$  on the grid resolution used in the analysis?
4. How well do microtopographic estimations of  $z_0$  compare with measured values of  $z_0$  from wind profile data?

## **2. Glacier surface energy balance and measurements of $z_0$**

Turbulent heat exchange between the air and a glacier surface is primarily driven by gradients of temperature and moisture in the lowermost 2-3 m of the atmosphere. Accurate and multiple measurements of temperature and humidity above the ice surface are rarely available, however, so for calculation of sensible and latent heat

fluxes the 'bulk' aerodynamic method is frequently applied (Hock, 2005). The bulk method requires only single measurements of wind speed, temperature and humidity, providing the  $z_0$  of the glacier surface is also known. Its accuracy is largely dependent on how well  $z_0$  can be specified; previous work has shown that it can vary over at least four orders of magnitude (Bintania and van den Broeke, 1994; Smeets et al., 1999; Brock et al., 2006). Despite this, surface energy balance studies regularly use a spatially- and temporally-invariant value to represent  $z_0$ , and often simply assume values based on data from previously published studies (e.g. Rounce and McKinney, 2014) rather than measuring or parameterising surface roughness using in situ observations. This can be problematic because direct measurements of  $z_0$  over glacierised surfaces are relatively sparse (cf. Table 1 in Brock et al., 2006), and are thus unlikely to be appropriate for multiple studies or dynamically-evolving surfaces. At least for debris-covered glacier surfaces measurements of  $z_0$  should not change radically during the melt season, with the primary controls of lithology, weathering and redistribution of the debris material remaining independent of the melting surface (Foster et al., 2012).

Very few direct measurements of  $z_0$  exist over debris-covered ice surfaces (Nield et al., 2012), with those that are available coming solely from vertical profiles of horizontal wind-speed measurements. Using this approach, wind speed is measured at two or more known heights above the glacier surface and  $z_0$  is defined by the intercept of a logarithmic profile fit through the data (Munro, 1989). Each profile represents a single wind 'event' during which wind speed is maintained above a threshold value for a set period of time, and data are adjusted to account for surface layer stability using Monin-Obukhov similarity theory (Stull, 1988). Previous work has shown that  $z_0$  values derived using this approach are very sensitive to the measured

height of each anemometer, and that the setup required for a reliable measurement is non-trivial (Munro, 1989; Wieringa, 1993; Smeets et al., 1999). Nonetheless, Brock et al. (2010) successfully used wind profile measurements to calculate a mean roughness length of 0.016 m for the Miage Glacier, Italy, and Takeuchi et al. (2000) similarly derived a value of 0.0063 m for the Khumbu Glacier, Nepal, albeit using only two anemometers and assuming, rather than confirming, neutral conditions in the latter case. Comparable values of 0.0035 m at the debris/clean-ice interface and 0.06 m over the debris-covered area of Khumbu Glacier were measured by Inoue and Yoshida (1980), but again only using two anemometers and assuming neutral conditions.

Other studies have adopted microtopographic approaches to estimate  $z_0$  (e.g. Smith et al., 2016) or tuned its value to fit other observations (e.g. Foster et al., 2012). The most commonly used microtopographic approach is based on the work of Lettau (1969), which describes roughness elements in terms of their height ( $h^*$ ) (m), their density, or frequency per unit area ( $S$ ) ( $m^2$ ), and their silhouette area ( $s$ ) ( $m^2$ ), all measured in a vertical plane perpendicular to wind direction:

$$z_0 = 0.5h^*s/S \quad (1)$$

The value of 0.5, commonly referred to as the drag coefficient, accounts for the change in effective drag by individual elements with increased relative sheltering (Wieringa, 1993). It is a first order correction and likely varies in reality (Garrett, 1977; Raupach, 1992), but in glaciological studies the value of 0.5 has been widely adopted (e.g. Brock et al., 2006; Rounce et al., 2015).

### **3. Site description and methods**

#### **3.1 Field site**

Khumbu Glacier is 15.7 km long and 26.5 km<sup>2</sup> in area and is located in the Everest region of Nepal (Figure 1). Debris covers the lowermost 8 km of ice (around 37% of the total glacier area; Soncini et al., 2016) and measures up to several metres thick in places (Nakawo et al., 1999). The lowermost 5 km of ice is stagnant (Rowan et al., 2015) and mass loss is predominantly through surface lowering (Bolch et al., 2011; King et al., 2016) rather than terminus recession, leading to a generally undulating surface topography pocked by surface ponds and associated ice-cliffs (Nuimura et al., 2011). A thin inceptisol is present over large parts of the true-right hand side of the glacier whereas a string of linked surface ponds dominates the lowermost few kilometres of the true-left side of the glacier (Watson et al., 2016).

We characterised roughness at two sites (Figure 1) on the surface of Khumbu Glacier during the post-monsoon season of 2015. Each site measured 15 m x 60 m and was orientated with the long axis parallel to glacier flow and the observed predominant wind direction. These two sites were chosen to be representative of the wider debris-covered glacier surface. The first site consisted of a sandy gravelly matrix (~ 99%) with discrete patches of cobbles measuring up to several tens of centimetres in diameter. Mean clast size was estimated to be of the order of millimetres to centimetres and small areas of scrub vegetation were observed. The second site consisted of cobbles and boulders overlying a silty sandy matrix in places but separated by voids for the most part. Estimated mean clast size was 50-100 mm and although vegetation was mostly absent some small patches of grass were observed to be growing between clasts.

Previous work has shown that wind direction and speed at the Khumbu Glacier follow diurnal and seasonal cycles (Bollasina et al., 2002). Strong up-glacier winds tend to prevail during the daytime, peaking between 12:00 and 14:00, and this

pattern is unaffected by any seasonal variation. In all seasons other than the summer monsoon, a night-time down-glacier wind is also present, peaking during 02:00 and 06:00 during the pre-monsoon period, which is coincident with our period of data collection (Bollasina et al., 2002).

### **3.2 Wind profile $z_0$ measurements**

We erected a wind tower at Site 1 for a period of five days, from October 22<sup>nd</sup> (morning) to October 27<sup>th</sup> (morning) and redeployed it at Site 2 for a further four days, from October 27<sup>th</sup> (morning) to October 30<sup>th</sup> (evening). The wind tower comprised five NRG #40 cup anemometers positioned at heights of 0.210, 0.765, 1.320, 1.875 and 2.445 metres above the surface (measured from a flat plate laid horizontally over the ground surface), one NRG 200P wind vane mounted on top of the mast, and five Tinytag TGP-4017 temperature loggers (manufacturer-stated accuracy < 0.01 °C) shielded from direct and longwave (reflected) radiation by naturally aspirated white plastic hose and mounted at the same height as the anemometers (Figure 2). We acknowledge that with this simple design there may be some systematic over- or under-estimation of the temperatures, but consider this to be minimal given the sensors are low in mass (Tarara and Hoheisel, 2007; Kurzeja, 2010). Wind instrument data were recorded at one minute intervals (averaged 60 s data) by a Campbell CR1000 logger, powered by a 12V rechargeable battery and housed in a padded lunchbox within a dry-bag at the foot of the tower. Temperature loggers recorded data internally, also at one minute intervals.

Following fieldwork, the temperature data were calibrated relative to a mean dataset derived from 12000 measurements under controlled conditions (4 °C). Adjustments ranged from -0.04 to +0.03 °C between loggers. Corrections to the instrument

heights above the surface were also made to account for changes in measured snow-depth during the observation period.

Aerodynamic roughness values were estimated by assuming the wind and temperature profiles were given by Monin-Obukhov (MO) similarity theory (see e.g. Stull, 1988). This includes an empirical-based modification of the classical logarithmic wind profile to account for the effects of stability. Before fitting the wind profiles the data were filtered. Any 60-second period where the lowermost mean wind speed was less than 1.0 m/s was not used since the cup anemometers have a stall speed of 0.7 m/s (NRG Systems, 2016). MO theory also assumes the conditions are stationary (i.e. there is no systematic change in the mean temperature or winds over the period) (Oke, 1987) so to avoid non-stationary periods any 60 second interval in which the temperature changed by more than 0.25 °C was also filtered out. This tended to occur around sunrise / sunset when rapid heating / cooling took place. For each remaining 60 second period, an ordinary least squares fit of the wind and temperature profiles to the theory was performed (Namikas et al., 2003), and since the profiles were coupled, an iterative approach was required. The converged profile fits gave an estimate of  $z_0$ . Only fits where the  $r^2$  values for both the wind and temperature profiles were greater than 0.99 were retained for further analysis (Nield et al., 2013), yielding a final aerodynamic roughness dataset comprising 389 independent measurements. We found that the inclusion of stability effects was important and led to a noticeably better fit to the wind profiles, and less variability in the derived values of  $z_0$ .

### **3.3. Topographic surveys**

Both sites were photogrammetrically surveyed using a Canon G11 Powershot digital camera (6 mega pixels) so that topographic data could be derived using Structure from Motion Multi-View Stereo (SfM-MVS). We defined a rectangle measuring 15 m in width by 60 m in length centred on the wind tower positions and installed a network of ground control points, marked by yellow spray paint, across each site. Ground control point positions were recorded using a Leica VIVA GS10 differential GPS and post-processed against base station data from Syangboche (SYBC) to a reported (post-processing software derived) accuracy of < 10 mm. We anticipate the real accuracy of the ground control data to be up to 20-30 mm owing to some discrepancy between the placement of the receiver on the point in the field and the placement of the markers in Agisoft Photoscan.

All images were acquired at a height of approximately 2 m above ground and with angular changes of < 20° to aid keypoint identification (Moreels and Perona, 2007). Camera pose was oblique to the glacier surface to avoid the doming effect that has been observed in models using exclusively vertical images (James and Robson, 2014). Site 1 was surveyed once, at the beginning of the observation period. The survey comprised 329 images, 35 ground control points (GCPs), and six check points. Site 2 was first surveyed on the 29<sup>th</sup> October following a snowfall event (401 images; 17 GCPs; 6 check points) and then again twenty-four hours later just prior to the site being decommissioned (229 images; 18 GCPs; 3 check points). It was then re-surveyed two weeks following decommission to provide a snow-free topography (422 images; 36 GCPs; 6 check points), under the assumption that the site had not changed from its initial (pre-snow) condition.

### **3.4 Estimation of $z_0$ by microtopography**

Point-cloud data were derived using Agisoft Photoscan Professional version 1.2.3. Georeferencing errors ranged between 0.029 and 0.033 m Root Mean Square Error (RMSE); check point errors ranged between 0.007 m and 0.033 m  $RMSE_z$ , albeit with only 3 surveyed positions in one of the cases (Table 1). We assumed that the primary control on prevailing wind direction was the large scale catchment topography such that it flowed directly up- or down-glacier, as was observed during the study period. Accordingly, we used CloudCompare 2.6.2 (Girardeau-Montaut, 2016) to divide each cloud into two 15 m x 30 m areas of interest, one located up-wind of the wind tower and the other down-wind of the tower (so that  $z_0$  could be calculated for the dominant wind direction), and rotated them such that the long-axis was orientated north (positive y-axis) for ease of computation. The clouds were manually cleaned to account for obviously spurious matches and divided again to generate twenty new patches of various size. So that we could test the effect of both patch size and fetch on the microtopographic estimates we derived patches of 1 m x 1 m through to 15 m x 15 m, at every 1 m interval, as well as patches measuring 5 m x 10 m, 5 m x 15 m, 5 m x 20 m, 5 m x 25 m and 5 m x 30 m. Finally, these patches were decimated to generate rasters with grid resolutions of 10 mm, 50 mm and 100 mm using the mean z value for each cell.

We tested three methods, all of which have been previously detailed in full in Smith et al. (2016; see section 3.4 and Table 1 therein). The first method, which has been widely adopted in previous glaciological studies (e.g. Rees and Arnold, 2006; Brock et al., 2006; Rounce et al., 2015), follows the approach of Munro (1989). The Lettau equation (1) is simplified by assuming that  $h^*$  can be represented by twice the standard deviation of elevations of the detrended profile ( $2\sigma_d$ , m), with the mean elevation set to 0. The frontal silhouette area is then calculated to be:

$$s = \frac{2\sigma_d X}{2f} \quad (2)$$

and the ground area occupied by each roughness element (so-called lot area),  $S$  ( $\text{m}^2$ ), is approximated as:

$$S = \left(\frac{X}{f}\right)^2 \quad (3)$$

The aerodynamic roughness length for a given profile then becomes:

$$z_0 = \frac{f}{X} (\sigma_d)^2 \quad (4)$$

Using this method (hereafter referred to as the ‘profile-based’ approach),  $z_0$  was calculated for every profile in both orthogonal directions for each plot. We report the mean values for each plot, for profiles taken perpendicular to the wind direction.

The second approach (hereafter referred to as the ‘raster-based’ approach) uses the full DEM dataset to calculate the frontal area,  $s$ , directly for each cardinal wind direction. The DEM is first detrended and sheltering is implicitly represented by including only frontal areas above the detrended zero plane. The planar plot area is then used as the ground area  $S$  and  $h^*$  is calculated as the mean deviation above the detrended plane. We report the calculated value for each plot in the appropriate wind direction.

The third approach (hereafter referred to as the ‘cloud-based’ approach) uses a filtered version of the full point cloud, sub-sampled using an octree approach (Meagher, 1982) to ensure uniform point density. Here,  $s$  is calculated as the number of normal vectors facing each cardinal direction. Points below the detrended plane and flat surfaces defined as having a normal vector greater than  $80^\circ$  from horizontal are not used in the estimation of  $s$ . The plot area,  $S$ , is approximated by the total

number of points in the cloud (approximating the 3-D surface area). Finally, the effective obstacle height is calculated as the mean height above the detrended plane of all points above that plane. Again, in this study we report the calculated value for each plot in the appropriate wind direction.

## **4. Results**

### **4.1 Weather station data**

During the ten day observation period, weather conditions were uniform for the first six days; winds were routinely anabatic during the daytime and katabatic at night (Figure 3). They were strongest during the day, regularly approaching  $5 \text{ m s}^{-1}$ , and weakest at night, fluctuating between 0 and  $2 \text{ m s}^{-1}$ . The temperature gradient with elevation was negative during the day, but inverted at night; the maximum recorded temperature was  $16.4^\circ\text{C}$  and the minimum recorded temperature was  $-12.5^\circ\text{C}$ . At approximately 1900 hrs on the 28th October, a weather front travelling northward deposited 90 mm (mean measured depth in five locations) of snow across the glacier surface and up-valley winds became dominant during both day and night. Wind speeds fluctuated between 0 and 5 m/s for the remainder of the measurement period, and there was no clear variation in temperature with elevation. When the site was finally decommissioned, at 1500 hrs on the 30<sup>th</sup> October, the snow cover had partially melted and its mean depth ( $n = 5$ ) was 60 mm.

### **4.2 Wind profile measurements of $z_0$**

Five discrete periods of wind were evident in our measured  $z_0$  data. While the wind tower was deployed at Site 1, winds were predominantly blowing up-glacier during the daytime and down-glacier during the night, so  $z_0$  measurements were allocated

to one of these two periods accordingly. At Site 2 the winds were more uniform both in strength and direction, but ground conditions were variable because of the snowfall event of 28<sup>th</sup> October. Opportunistically, we used the natural variability of the ground conditions as an experiment to explore the influence of the microtopography on measured and estimated roughness values. We thus allocated the  $z_0$  measurements at Site 2 to one of three periods: a) no snow (i.e. before the snowfall began), b) full snow (for measurements acquired within 24 hours of the snowfall), and c) part snow (for measurements acquired > 24 hours after the snowfall and until the end of the measurement period).

Median  $z_0$  measurements for Site 1 (day = 0.0182 m; night = 0.0177 m) were lower than those for Site 2 prior to the snowfall event (0.0227 m), and this is reflected in the spread of the data, with Site 2 showing greatest variability in the estimated values (Table 2 and Figure 4). Following snowfall, the median  $z_0$  measurement for Site 2 dropped by almost an order of magnitude (0.0052 m) before increasing again following the period of melt (0.0126 m). Mean values were marginally higher in each case, reflecting the general spread of the data, but the pattern between sites remained the same. Part of the scatter in the data can be accounted for by non-uniform wind direction, with measured roughness lengths tending to increase as winds move round towards the west in each late afternoon period (Figure 5).

### **4.3 Microtopographic estimates of $z_0$**

Calculated  $z_0$  values varied between methods and between sites (Figure 6). At Site 1, there was good agreement between the three approaches. The profile-based method generally produced higher values of  $z_0$  than the raster and cloud-based methods when larger patch sizes were used but, even in the worst case, the

difference between the approaches was  $< 0.01$  m. The raster and cloud-based methods produced remarkably similar values of  $z_0$  regardless of the patch size. At Site 2, there was greater variability between the methods, with the cloud-based approach consistently producing the lowest values of  $z_0$  in each case. The raster-based method generally produced the highest  $z_0$  values, and the greatest difference between the methods was 0.045 m. Generally speaking, the profile and raster-based approaches showed the greatest similarity.

In almost all cases, the effect of taking the measurement over a larger area was to increase the calculated  $z_0$  value (Figure 6). At Site 1, the increase was relatively uniform whereas at Site 2 there was greater variability, with the profile method producing notably lower roughness values when using large patch sizes under full snow conditions. Of the three methods, the cloud-based approach appeared to be most stable, with calculated values increasing steadily with plot size. The profile-based method was the most unstable, showing greatest variability between plots of different size. The range of values produced by each method was lowest in the case of the cloud-based approach (0.024 m; Site 2 no snow) and highest in the case of the raster-based approach (0.056 m; Site 2 full snow).

Increasing the fetch (patch length) but retaining a constant width had only a small impact on the calculated values (Figure 6). Consistency between the approaches was improved, with the maximum disparity for any given patch size being 0.025 m, and generally  $< 0.015$  m. The profile-based method showed greatest consistency across the different patch sizes, with the range of values being  $< 0.01$  m in all cases. The raster-based approach showed greatest variability with increasing patch size, with values varying by  $> 0.025$  m in the most extreme case. There was no clear relationship between patch length and calculated  $z_0$  for any of the methods, with

values fluctuating around a mean value roughly comparable with that produced using the 5x5 m patch.

The general pattern of  $z_0$  values calculated using the profile and raster-based approaches was replicated at all sites, regardless of the resolution of the data (Figure 7). Without exception, the impact of decreasing data resolution was to reduce the calculated  $z_0$  value, although the effect was diminished as the data became increasingly coarse. The impact on the calculated  $z_0$  values was greatest when applying the raster-based method, with those values derived using the finest resolution (1 cm) data being more than double those from data gridded at 5 cm in all cases. Values calculated using the profile-based method appeared to be more stable, differing by just 0.016 m between the finest and coarsest resolution data in the worst case (Site 2 no snow). When compared to the aerodynamic data  $z_0$  was generally underestimated for the largest plots at Site 1, and overestimated for the largest plots at Site 2. The finest resolution data most closely replicated the aerodynamic values measured at Site 1, whereas the coarsest resolution data most closely replicated the aerodynamic values measured at Site 2. No resolution effect could be identified for the cloud-based approach since the calculations were made directly from the full resolution point cloud.

To compare the results produced by each method with those derived using the aerodynamic data, we plotted calculated vs. measured  $z_0$  values for each site using a resolution of 1 cm for both the 15m x 15m plot (Figure 8) and 5m x 5m plots (Figure 9). For the larger plot area at Site 1, all three methods generated roughness values comparable with those measured aerodynamically, and all three methods characterised the patch up-glacier of the wind tower (night) to be marginally rougher than the patch located down-glacier of the tower (day). All three methods produced

much higher  $z_0$  values for the snow-free period at Site 2, as was indicated also by the wind tower data, but the calculated profile and raster-based values exceeded the measured aerodynamic value by 0.020 m and 0.031 m respectively whereas the cloud-based method underestimated it by  $< 0.001$  m. The profile and raster-based methods grossly overestimated the measured roughness values for the periods with full and partial snow-cover, with the raster-based method even indicating a slight increase in roughness following the snowfall event. The cloud-based method slightly overestimated the measured tower values for the fully snow-covered period but produced values within 0.010 m of the measured values for all periods at Site 2. Only the cloud-based method yielded the same relative order of roughness values for the different sites as the aerodynamic measurements. For the smaller plot area (Figure 9) the profile and cloud based approaches consistently underestimated the measured aerodynamic values, whereas the raster based approach overestimated it at Site 2 following the snowfall event. As with the larger plots, only the cloud based approach replicated the relative ordering of roughness values between sites.

## 5. Discussion

The aerodynamic values measured in the present study are slightly higher than those previously reported in the literature (e.g. 0.001–0.01 m (Lettau, 1969)) but very similar to those measured by Brock et al. (2010) over debris-covered ice in the Italian Alps (0.016 m), as well as over shallow and deep crevasses on clean-ice surfaces (0.009–0.020 m) measured by Smith et al. (2016), and mixed rock-armoured and vegetated desert surfaces (0.009–0.024 m) measured by MacKinnon et al. (2004). It should be noted that the construction of a stable wind-tower or eddy-covariance station on often-mobile glacier surfaces is a challenging task, and establishing the ground surface level,  $z$ , plays a critical role in determining the  $z_0$  value from wind

velocity data (Munro, 1989). Variability in  $z$  of just 0.1 m can change the calculated  $z_0$  value by an order of magnitude, meaning values calculated over debris-covered surfaces, where the ground level is spatially heterogeneous, cannot be taken to be absolute. In addition, the derivation of  $z_0$  values from wind tower data generally requires a large homogeneous fetch (Wieringa, 1993), and debris-covered glacier topography is rarely homogeneous. Nevertheless, the order of our  $z_0$  values is in line with our field observations; Site 2 was visibly rougher than Site 1, and the roughness of Site 2 was reduced by the snow event before returning to its original state after several days of melting. This suggests that at least the relative accuracy of our wind-profile derived estimates of  $z_0$  is high.

The impact of wind direction on our calculated  $z_0$  values is interesting to note (Figure 5), and also provides evidence that our wind profile data are sound. Field observations recorded that the surface relief was anisotropic, with broad-scale undulations (ridges and furrows) aligned predominantly parallel to the glacier flow direction (Figures 2b and 2c). Roughness values calculated from winds blowing directly up- and down-glacier were consistently lower than those calculated as the wind direction became increasingly oblique to the ice-flow direction. These data emphasise that  $z_0$  values calculated from wind tower data are highly dependent on the wind direction, but also suggest that the broad-scale topography is particularly important in determining the roughness length, rather than the size and shape of individual obstacles, since surface debris appears to be, at least visually, randomly distributed.

The impact of the snow event on measured  $z_0$  values at Site 2 is also interesting in this regard. The snowfall event was sufficient to conceal the surface micro-topography, but did not alter the broad-scale topography or the existence of large

obstacles. The impact of snowfall on the aerodynamic roughness length was to reduce it by ~75%. Figure 2f shows the relative smoothing of the surface under full, part and no snow conditions. This natural experiment reveals that the microtopography plays a very important role in controlling near-surface airflow. Lithology, weathering and debris distribution have all been previously cited as being important controls of  $z_0$  variability (Foster et al., 2012). Our findings suggest that debris distribution is also important, but perhaps on a much smaller scale than has previously been acknowledged. Our results also suggest that while the often-used  $z_0$  value of 0.016 m holds for debris-covered surfaces comprising gravels and cobbles, as at Site 1, a value of 0.020-0.025 m may be more appropriate for debris-covers consisting of cobbles and boulders. For even rougher surfaces, comprising mostly boulders for example, a value  $> 0.03$  m may be most representative (Inoue and Yoshida, 1980), although at this scale subsurface airflows may also begin to play an important role (Evatt et al., 2015).

The microtopographic values calculated here fluctuated with the both the size and resolution of the patch, typically underestimating  $z_0$  with small patch sizes and coarse resolution data, and often overestimating it with large patch sizes and fine resolution data, at least when compared to the wind tower values. At Site 1, the microtopographic values were comparable to those generally used for debris-covered ice in the literature (*cf.* Rounce and McKinney, 2014; Foster et al., 2012) but at Site 2 the profile and raster-based methods produced values considerably higher than those that have been used elsewhere. The range in our microtopographic data varied with the plot size, measurement resolution and method (Supplementary S1), suggesting that studies without independent measurements of aerodynamic  $z_0$  should treat microtopographic estimates with caution.

Brock et al. (2006) found that when using the profile method the length of the transect over which they took their measurements had little impact on the calculated value (no statistically significant difference between 3 m and 9 m profiles and no systematic variation up to 15 m in length). This is perhaps surprising since microtopographic and aerodynamic measures of roughness are known to be scale-dependent (Sun et al., 2016), and also sensitive to fetch (Peterson et al., 1978). For example, using a combination of LiDAR and fine-scale microtopographic measurements collected over midre Lovénbreen, Svalbard, Rees and Arnold (2006) suggested scale dependence of  $z_0$  existed within a region of 70-500 mm in horizontal extent and 6-70 mm vertically. In terms of fetch, Wieringa (1993) showed that aerodynamic measurements of surface roughness may be affected by topographic elements situated at a horizontal distance two orders of magnitude greater than the observation height.

In our case, estimated  $z_0$  values were noticeably more dependent on plot width than plot length (Figure 6), which is likely to reflect the generally convex cross-plot topographies at both sites (Figure 2). The non-linearity of the transverse profiles inflated  $h^*$  in the profile approach in particular, resulting in an artificially high estimate of  $z_0$ . In areas of high relief it may therefore be that the linear/planar detrends applied to profiles/plots here and in previous studies are inappropriate and that a scale-dependent or spatially variable (e.g. coarse-DEM removal or quadric surface) correction should be applied. This becomes a particularly important consideration for raster- and cloud-based approaches that require a three-dimensional transform and where the topography is likely to incorporate greater heterogeneity. The microtopographic estimates were only slightly dependent on plot length (or equally, fetch). Notably estimates of  $z_0$  at site 2 derived using the profile- and raster-based

methods compared well with those derived using the cloud-based method and the wind-tower data over both long and short fetches. This is likely to be a product of the relatively uniform topography in a direction parallel to glacier flow at both sites.

Without exception, the impact of increasing data resolution was to increase the estimated  $z_0$  values. This is perhaps unsurprising; degrading the resolution of the data has a similar impact to running a low-pass filter over it, or indeed covering it with a thin layer of snow (Figure 2f), removing the high spatial frequency detail. These data confirm that capturing surfaces in fine resolution is crucial if roughness proxies are to be robustly employed. Similar conclusions have been reached in other disciplines; for example Darby et al. (2010) characterised surface roughness values at a riverbank on the Cecina River in Italy using multi-resolution point-cloud data finding that the estimated roughness values were positively correlated with cloud density. This effect appears only to be evident up to a point in our data, however, with the  $z_0$  values calculated using 50 mm resolution data only differing slightly from those calculated using 100 mm data. It is likely that convergence to a scale-independent  $z_0$  value would also be seen at finer resolutions, and implies that it is important to characterise the fine surface detail when adopting microtopographic approaches. It also confirms that previous simplified approaches using sparse measurements of surface elevation with respect to a horizontal datum (as proposed by Munro, 1989) are likely to have underestimated the true roughness value (MacDougall and Flowers, 2011).

Across sites, the cloud-based approach correlated most closely with the aerodynamic  $z_0$  values derived from the wind-tower data. There was noticeable disparity between the cloud-based approach and the profile- and raster-based approaches in the current study, particularly at the larger plot sizes. Smith et al.

(2016) reported good agreement between the three approaches, but only using smaller (2 m x 2 m) plots, at which scale our data also show good agreement even if they underestimate  $z_0$  in each case. Our full dataset (Supplementary data S1) confirms that the profile-based method produces highly variable results even within a single plot (as noted by Irvine-Fynn et al., 2014), and is direction dependent. There is an argument for integrating profiles both parallel and perpendicular to flow so that frontal areas from opposing wind directions can be resolved (i.e. where roughness is anisotropic), and this holds even for debris-covered ice surfaces where the larger scale topography is dynamically (i.e. driven by ice flow) as well as aerodynamically dependent.

Although in the current study all of the microtopographic estimates of  $z_0$  consistently underestimated the absolute values derived using the wind tower data at smaller plot sizes, their relative accuracy suggests they may still hold some value (Figure 9). It is possible that with the smaller plot sizes some obstacles outside the survey area were not captured, and/or that the role of the broad-scale topography was neglected. We also note, however, that the drag coefficient of Lettau (1969) was not derived empirically; rather it was proposed as an 'average' effect of form drag on an individual obstacle. This may hold for relatively homogeneous topographies, but perhaps breaks down in more complex situations. On a debris-covered glacier, for example, drag may be high given the density and irregular shape of the topographic elements, and a value of 0.7-0.8 may be more appropriate (*cf.* Figure 32 in Hoerner, 1965). The appropriateness of a single, catch-all, drag coefficient in the context of glacier surfaces may therefore be an appropriate focus for further research, as might a reanalysis of detrending methods for such complex terrains.

The broader implications of these findings are that microtopographic estimates of  $z_0$  should be used with caution, both in debris-free and debris-covered glacial settings, and most likely in other non-glacial environments too. They represent a further step towards developing a robust strategy for modelling melt under a debris-layer (Lejeune et al., 2013; Nicholson and Benn, 2013), although exactly how important turbulent fluxes are for melt at the ice-debris interfaces remains poorly constrained (Rounce et al., 2015). From a modelling point of view, there are equally big challenges in parameterising the rate of heat conduction through the debris and how this is influenced by moisture and water flow (Reid and Brock, 2010; Collier et al., 2014), determining the importance of changing albedo with debris continuity (Reid and Brock, 2012), and quantifying the effects of wind-driven evaporation inside the debris layer (Evatt et al., 2015), to name a few. Ultimately, the possibility that field measurements of surface roughness may be related to backscatter properties collected by airborne and satellite radar is an exciting prospect (Rees and Arnold, 2006) and one which might eventually lead to the up-scaling of field measurements of roughness to the glacier, or even regional scale (Greeley et al., 1988). Such an advance would represent a genuine breakthrough in efforts to model regional cryospheric response to a changing climate.

## **6. Conclusions**

This study tested three methods of calculating surface roughness using microtopographic data and compared the results to simultaneously acquired aerodynamic measurements. The aerodynamic data suggest that the often-used  $z_0$  value of 0.016 m is only suitable for homogeneous sites comprising sands, gravels and cobbles, and that values of  $> 0.020$  m are more appropriate for sites comprising larger clasts that are commonly found on debris-covered glaciers in the Himalaya

(e.g. Rounce et al., 2015). They also revealed, through the analysis of measurements over full, part and no snow conditions, that the microtopography of the terrain plays an important role in controlling near-surface airflow.

There was great variability in each of the microtopographic methods that were used, suggesting that future work should treat estimates derived from such approaches with caution. The profile-based method that has commonly been used in glaciological studies performed well where obstacles were small and homogeneous, but less well where the surface comprised clasts of mixed size and shape. The fully three-dimensional approach developed by Smith et al. (2016) was the only method to replicate the relative order of roughness between sites and also showed the greatest stability over different resolutions and plot sizes. Nevertheless, all three approaches showed scale-dependence, both in terms of the survey plot size and the data resolution, and although no clear thresholds were evident in our work to indicate the ideal survey setup, larger plot sizes (> 5 m x 5 m) characterised at the finest resolution (10 mm) were consistently closest to the measured aerodynamic values.

We suggest that further consideration of the drag coefficient used in most topographic estimates of roughness (i.e. its appropriateness for heterogeneous and angular debris-covered surfaces), and the testing of alternative detrending methods (e.g. quadric or coarse-DEM surface), may be fruitful areas for future related research.

## **7. Acknowledgements**

The authors would like to acknowledge the provision of the dGPS by the NERC Geophysical Equipment Facility (loan numbers 1050, 1058 and 1065), and thank the GEF Edinburgh staff for assistance before and during fieldwork in setting up the

equipment. Field logistics were provided by Himalayan Research Expeditions, and thanks go to our guides, Mahesh Magar and Dev, for their support. Phil Porter wrote the CR-1000 logger programme, for which we are grateful, and Ann Rowan provided useful direction and suggestions in the field. We thank two anonymous reviewers who provided detailed comments that helped to improve the quality of the final manuscript.

## **8. References**

Arnold NS, Rees WG. 2003. Self-similarity in glacier surface characteristics. *Journal of Glaciology* 49: 547-554.

Benn DI, Bolch T, Hands K, Gulley J, Luckman A, Nicholson LI, Quincey DJ, Thompson S, Toumi R, Wiseman S. 2012. Response of debris-covered glaciers in the Mount Everest region to recent warming, and implications for outburst flood hazards. *Earth-Science Reviews* 114: 156-174.

Bintanja R, van den Broeke MR. 1994. Local climate, circulation and surface-energy balance of an Antarctic blue-ice area. *Annals of Glaciology* 20: 160–168.

Bolch T, Pieczonka T, Benn DI. 2011. Multi-decadal mass loss of glaciers in the Everest area (Nepal Himalaya) derived from stereo imagery. *The Cryosphere* 5(2): 349-358.

Bollasina M, Bertolani L, Tartari G. 2002. Meteorological Observations at High Altitude in the Khumbu Valley, Nepal Himalayas, 1994-1999. *Bulletin of Glaciological Research* 19: 1-11.

Brock BW, Willis IC, Sharp MJ. 2006. Measurement and parameterization of aerodynamic roughness length variations at Haut Glacier d'Arolla, Switzerland. *Journal of Glaciology* 52: 281–297.

Brock BW, Mihalcea C, Kirkbride MP, Diolaiuti G, Cutler MEJ, Smiraglia C. 2010. Meteorology and surface energy fluxes in the 2005–2007 ablation seasons at the Miage debris-covered glacier, Mont Blanc Massif, Italian Alps. *Journal of Geophysical Research* 115: D09106.

Chappell A, Heritage GL. 2007. Using illumination and shadow to model aerodynamic resistance and flow separation: An isotropic study. *Atmospheric Environment* 41: 5817–5830.

Collier E, Nicholson LI, Brock BW, Maussion F, Essery R, Bush AB. 2014. Representing moisture fluxes and phase changes in glacier debris cover using a reservoir approach. *The Cryosphere* 8(4):1429-44. Darby SE, Trieu HQ, Carling PA, Sarkkula J, Koponen J, Kumm M, Conlan I, Leyland J. 2010. A physically based model to predict hydraulic erosion of finegrained riverbanks: the role of form roughness in limiting erosion. *Journal of Geophysical Research* 115: F04003.

Eitel JUH, Williams CJ, Vierling LA, Al-Hamdan OZ, Pierson FB. 2011. Suitability of terrestrial laser scanning for studying surface roughness effects on concentrated flow erosion processes in rangelands. *Catena*, 87(3): 398-407.

Evatt GW, Abrahams ID, Heil M, Mayer C, Kingslake J, Mitchell SL, Fowler AC, Clark CD. 2015. Glacial melt under a porous debris layer. *Journal of Glaciology* 61(229): 825-36.

Foster LA, Brock BW, Cutler MEJ, Diotri F. 2012. A physically based method for estimating supraglacial debris thickness from thermal band remote-sensing data. *Journal of Glaciology* 58(210): 677-691.

Garratt JR. 1977. Review of drag coefficients over oceans and continents. *Monthly Weather Review* 105: 915–929.

Girardeau-Montaut D. 2016. CloudCompare - Open Source Project. <http://www.danielgm.net/cc/> (accessed 5 November 2016).

Greeley R, Lancaster N, Sullivan RJ, Saunders RS, Theilig E, Wall S, Dobrovolskis A, White BR, Iversen JD. 1988. A relationship between radar backscatter and aerodynamic roughness: Preliminary results. *Geophysical Research Letters* 15(6): 565-568.  
Hock R. 2005. Glacier melt: A review of processes and their modelling. *Progress in Physical Geography* 29(3): 362–391.

Hock R, Holmgren B. 1996. Some aspects of energy balance and ablation of Storglaciären, northern Sweden. *Geografiska Annaler* 78A(2–3): 121–131.

Hoerner SF. 1965. Fluid-dynamic drag. Bricktown, NJ: Published by the author.

Inoue J, Yoshida M. 1980. Ablation and heat exchange over the Khumbu glacier. Seppyo, *Journal of the Japanese Society of Snow and Ice* 41: 26–33.

Irvine-Fynn TDL, Sanz-Ablanedo E, Rutter N, Smith MW, Chandler JH. 2014. Measuring glacier surface roughness using plot-scale, close-range digital photogrammetry. *Journal of Glaciology* 60: 957–969.

James MR, Robson S. 2014. Mitigating systematic error in topographic models derived from UAV and ground-based image networks, *Earth Surface Processes and Landforms* 39: 1413–1420.

King O, Quincey DJ, Carrivick JL, Rowan AV. 2016. Spatial variability in mass change of glaciers in the Everest region, central Himalaya, between 2000 and 2015. *The Cryosphere Discussions*: 1-35.

Kurzeja R. 2010. Accurate temperature measurements in a naturally-aspirate radiation shield. *Boundary-Layer Meteorology* 134:181-193.

Lejeune Y, Bertrand JM, Wagnon P, Morin S 2013. A physically based model of the year-round surface energy and mass balance of debris-covered glaciers. *Journal of Glaciology* 59(214): 327–344.

Lettau HH. 1969. Note on aerodynamic roughness parameter estimation on the basis of roughness element description. *Journal of Applied Meteorology* 8: 828–832.

MacDougall AH, Flowers GE. 2011. Spatial and temporal transferability of a distributed energy-balance glacier melt model. *Journal of Climate* 24(5): 1480-1498.

MacKinnon DJ, Clow GD, Tigges RK, Reynolds RL, Chavez PS. 2004. Comparison of aerodynamically and model-derived roughness lengths ( $z_0$ ) over diverse surfaces, central Mojave Desert, California, USA. *Geomorphology* 63(1): 103-13.

Meagher D. 1982. Geometric modelling using octree encoding, *Computer Graphics and Image Processing* 19: 129–147.

Moreels P, Perona P. 2007. Evaluation of features detectors and descriptors based on 3D objects. *International Journal of Computer Vision* 73(3): 263–284.

Munro DS. 1989. Surface roughness and bulk heat transfer on a glacier: Comparison with eddy correlation. *Journal of Glaciology* 35(121): 343–348.

Nakawo M, Yabuki H, Sakai A. 1999. Characteristics of Khumbu Glacier, Nepal Himalaya: recent changes in the debris covered area. *Annals of Glaciology* 28: 118–122.

Namikas SL, Bauer BO, Sherman DJ. 2003. Influence of averaging interval on shear velocity estimates for aeolian transport modeling. *Geomorphology* 53: 235–246.

Nicholson L, Benn DI. 2006. Calculating ice melt beneath a debris layer using meteorological data. *Journal of Glaciology* 52(178): 463-470.

Nicholson L, Benn DI. 2013. Properties of natural supraglacial debris in relation to modelling sub-debris ice ablation. *Earth Surface Processes and Landforms* 38(5): 490-501.

Nield JM, King J, Wiggs GFS, Leyland J, Bryant R, Chiverrell RC, Darby SE, Eckardt FD, Thomas DSG, Vircavs LH, Washington R. 2013. Estimating aerodynamic roughness over complex surface terrain. *Journal of Geophysical Research - Atmospheres* 118: 12,948–12,961.

Nield JM, Chiverrell RC, Darby SE, Leyland J, Vircavs LH, Jacobs B. 2012. Complex spatial feedbacks of tephra redistribution, ice melt and surface roughness modulate ablation on tephra covered glaciers. *Earth Surface Processes and Landforms* 38(1): 95–102.

NRG Systems, 2016. Specifications of the NRG #40C anemometer. <https://www.renewablenrgsystems.com/products/meters/sensors/anemometers/detail/40c-anemometer>

Nuimura T, Fujita K, Fukui K, Asahi K, Aryal R, Ageta Y. 2011. Temporal changes in elevation of the debris-covered ablation area of Khumbu Glacier in the Nepal Himalaya since 1978. *Arctic, Antarctic, and Alpine Research* 43(2): 246-55.

Oke TR. 1987. *Boundary Layer Climates*. Routledge: London.

Østrem G. 1959. Ice melting under a thin layer of moraine, and the existence of ice cores in moraine ridges. *Geografiska Annaler* 41(4): 228–230.

Peterson EW, Jensen NO, Kristensen L, Lundtang Petersen E, Højstrup J, Busch NE. 1978. The effect of local terrain irregularities on the mean wind and turbulence characteristics near the ground. *Proceedings of the Papers Presented at the WMO Symposium on Boundary Layer Physics Applied To Specific Problems of Air Pollution*: 45-50.

Racoviteanu AE, Arnaud Y, Williams MW, Ordonez J. 2008. Decadal changes in glacier parameters in the Cordillera Blanca, Peru, derived from remote sensing. *Journal of Glaciology* 54(186): 499-510.

Raupach MR. 1992. Drag and drag partition on rough surfaces. *Boundary-Layer Meteorology* 60: 375–395.

Rees WG, Arnold NS. 2006. Scale-dependent roughness of a glacier surface: implications for radar backscatter and aerodynamic roughness modelling. *Journal of Glaciology* 52(177): 214-222.

Reid TD, Brock BW. 2010. An energy-balance model for debris-covered glaciers including heat conduction through the debris layer. *Journal of Glaciology* 56(199): 903-16.

Reid TD, Carenzo M, Pellicciotti F, Brock BW. 2012. Including debris cover effects in a distributed model of glacier ablation. *Journal of Geophysical Research: Atmospheres* 117: D18. Röhl K. 2008. Characteristics and evolution of supraglacial ponds on debris-covered Tasman Glacier, New Zealand. *Journal of Glaciology* 54(188): 867-880.

Rounce DR, Quincey DJ, McKinney DC. 2015. Debris-covered energy balance model for Imja-Lhotse Shar Glacier in the Everest region of Nepal. *The Cryosphere Discussions* 9: 3503-3540.

Rounce DR, McKinney DC. 2014. Debris thickness of glaciers in the Everest area (Nepal Himalaya) derived from satellite imagery using a nonlinear energy balance model. *The Cryosphere* 8(4): 1317-1329.

Rowan AV, Egholm DL, Quincey DJ, Glasser NF. 2015. Modelling the feedbacks between mass balance, ice flow and debris transport to predict the response to climate change of debris-covered glaciers in the Himalaya. *Earth and Planetary Science Letters* 430: 427-438.

Scherler D, Bookhagen B, Strecker MR. 2011. Spatially variable response of Himalayan glaciers to climate change affected by debris cover. *Nature Geoscience* 4(3): 156-159.

Smeets CJPP, Duynkerke PG, Vugts HF. 1999. Observed wind profiles and turbulence fluxes over an ice surface with changing surface roughness. *Boundary-Layer Meteorology* 92(1): 99-121.

Smith MW, Cox NJ, Bracken LJ. 2011. Terrestrial laser scanning soil surfaces: a field methodology to examine surface roughness and overland flow hydraulics. *Hydrological Processes* 25: 842–860.

Smith MW, Quincey DJ, Dixon T, Bingham RG, Carrivick JL, Irvine-Fynn TD, Rippin DM. 2016. Aerodynamic roughness of glacial ice surfaces derived from high-resolution topographic data. *Journal of Geophysical Research: Earth Surface* 121(4): 748-766.

Soncini A, Bocchiola D, Confortola G, Minora U, Vuillermoz E, Salerno F, Viviano G, Shrestha D, Senese A, Smiraglia C, Diolaiuti G. 2016. Future hydrological regimes and glacier cover in the Everest region: The case study of the upper Dudh Koshi basin. *Science of the Total Environment* 565: 1084–1101.

Stull RB. 1988. *An Introduction to Boundary-Layer Meteorology*. Springer Netherlands.

Sun G, Hu Z, Wang J, Xie Z, Lin Y, Huang F. 2016. Upscaling analysis of aerodynamic roughness length based on in situ data at different spatial scales and remote sensing in north Tibetan Plateau. *Atmospheric Research* 176: 231-239.

Takeuchi Y, Kayastha RB, Nakawo M. 2000. Characteristics of ablation and heat balance in debris-free and debris-covered areas on Khumbu Glacier, Nepal Himalayas, in the pre-monsoon season. *IAHS Publication*: 53-62.

Tarara JM, Hoheisel GA. 2007. Low-cost shielding to minimize radiation errors of temperature sensors in the field. *HortScience* 42(6):1372-1379.

Thompson S, Benn DI, Mertes J, Luckman A. 2016. Stagnation and mass loss on a Himalayan debris-covered glacier: processes, patterns and rates. *Journal of Glaciology* 62(233): 467-485.

Watson CS, Quincey DJ, Carrivick JL, Smith MW. 2016. The dynamics of supraglacial ponds in the Everest region, central Himalaya. *Global and Planetary Change* 142: 14-27.

Wieringa J. 1993. Representative roughness parameters for homogeneous terrain. *Boundary Layer Meteorology* 63: 323–363.

Accepted Article

Table 1: Georeferencing and checkpoint errors for each full point cloud. Note that with the exception of ‘Site 2 part snow’, each of the clouds was then divided into up-glacier and down-glacier segments so that different surface roughness values could be computed depending on wind direction.

Site	Size of cloud	Georeferencing (RMSE)					Checkpoints (RMSE <sub>z</sub> )	
		n	X (m)	Y (m)	Z (m)	Total (m)	n	Total (m)
1	15 m x 60 m	35	0.025	0.018	0.011	0.033	6	0.033
2 (no snow)	15 m x 60 m	36	0.025	0.020	0.010	0.034	6	0.024
2 (full snow)	15 m x 60 m	17	0.024	0.019	0.006	0.031	6	0.013
2 (part snow)	15 m x 30 m*	18	0.021	0.015	0.011	0.029	3	0.007

\*only down-glacier area surveyed before weather deteriorated

Table 2: summary statistics of  $z_0$  values for each site

Site	Median (m)	Mean (m)	Min (m)	Max (m)	St. dev (m)
Site 1 day	0.0182	0.0184	0.0026	0.0423	0.0064
Site 1 night	0.0177	0.0195	0.0078	0.0402	0.0085
Site 2 no snow	0.0227	0.0243	0.0015	0.0560	0.0109
Site 2 full snow	0.0052	0.0055	0.0019	0.0118	0.0031
Site 2 part snow	0.0126	0.0129	0.0029	0.0294	0.0067

Accepted Article



Figure 1: The Khumbu Glacier, imaged by the ALOS AVNIR on 24 October 2008, showing its national context (inset) and the location of the two field sites (indicated in yellow). Eastings and northings are in metres according to UTM WGS84 Zone 45.

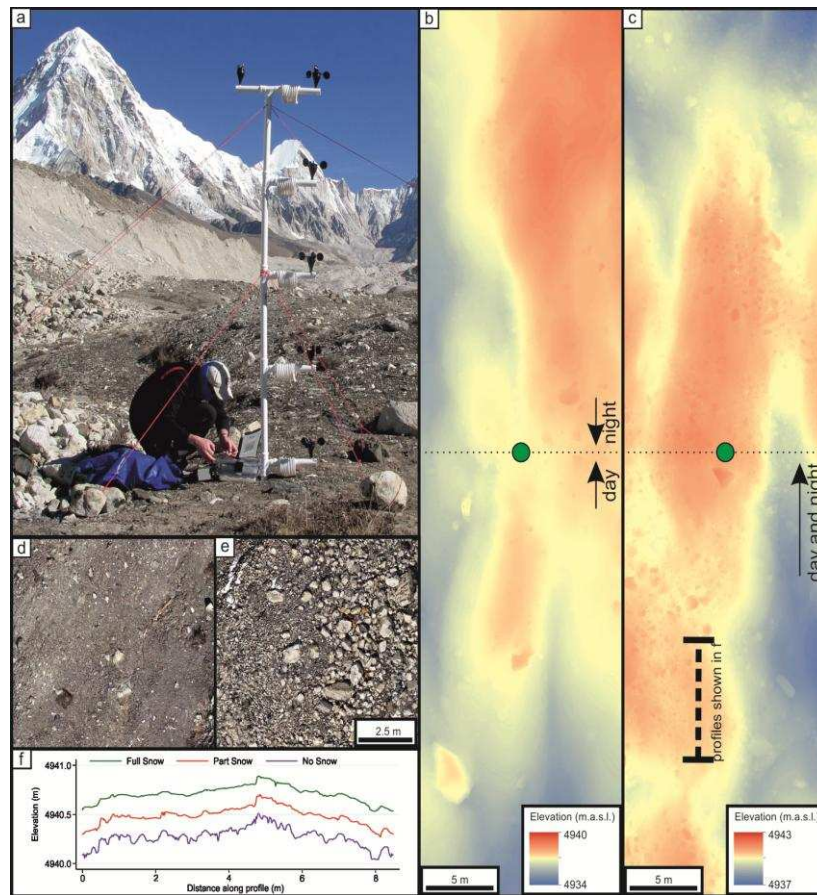


Figure 2: a) the wind tower in operation at Site 1, comprising a wind vane, five anemometers, five temperature loggers shielded from direct radiation by white plastic hose, and a Campbell CR1000 logger housed in a padded box in the drybag at the foot of the tower. b) Full DEM of Site 1 displayed at 0.01 m resolution (green circle denotes tower location and predominant wind directions are given). c) Full DEM of Site 2 displayed at 0.01 m resolution (green circle denotes tower location and predominant wind direction is given). d) Typical surface cover at Site 1 (plot dimensions are 10 m x 10 m). e) Typical surface cover at Site 2 (plot dimensions are 10 m x 10 m). f) Surface elevations extracted from profile shown in c). Note part-snow and no-snow profiles have been lowered by 0.2 m and 0.4 m respectively to aid clarity.

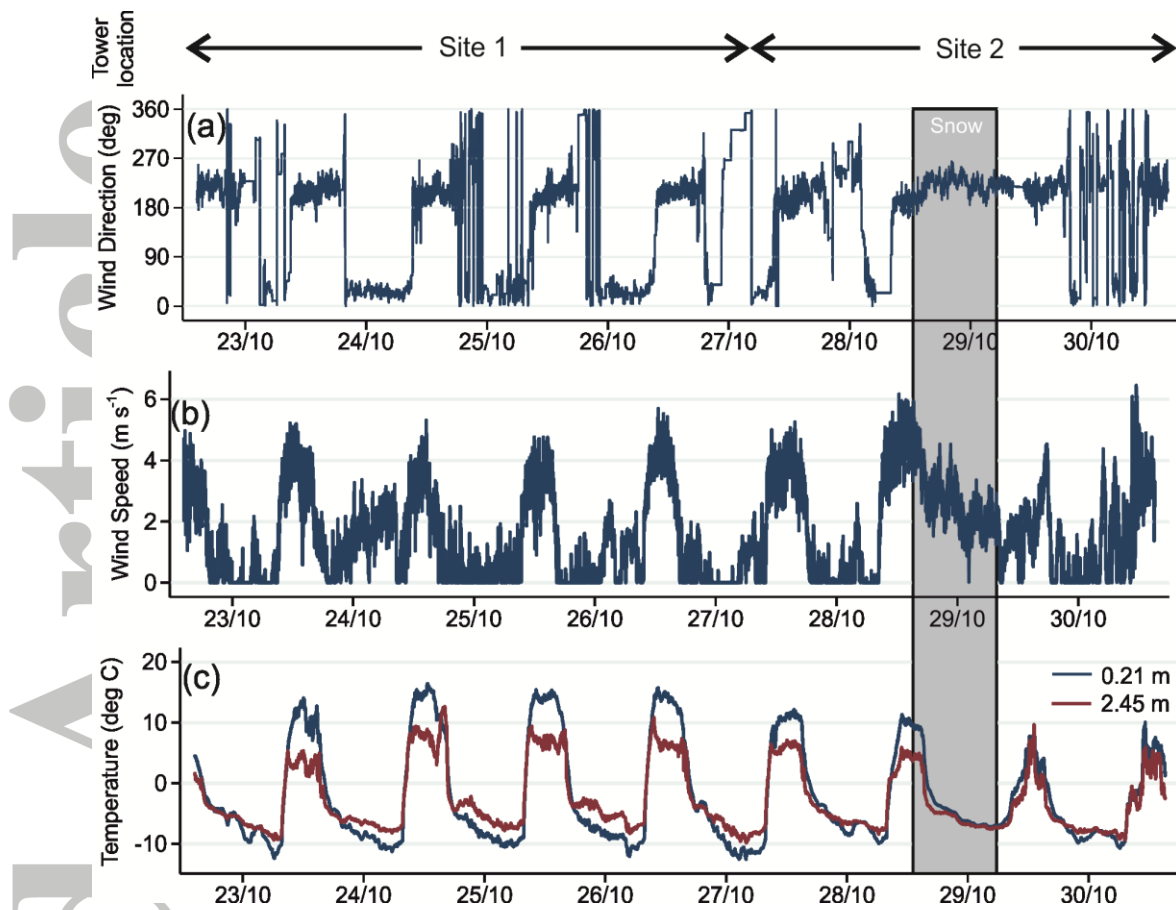


Figure 3: full suite of wind tower data for the observation period showing a) wind direction b) average wind speed, and c) temperature at the uppermost and lowermost anemometer height.

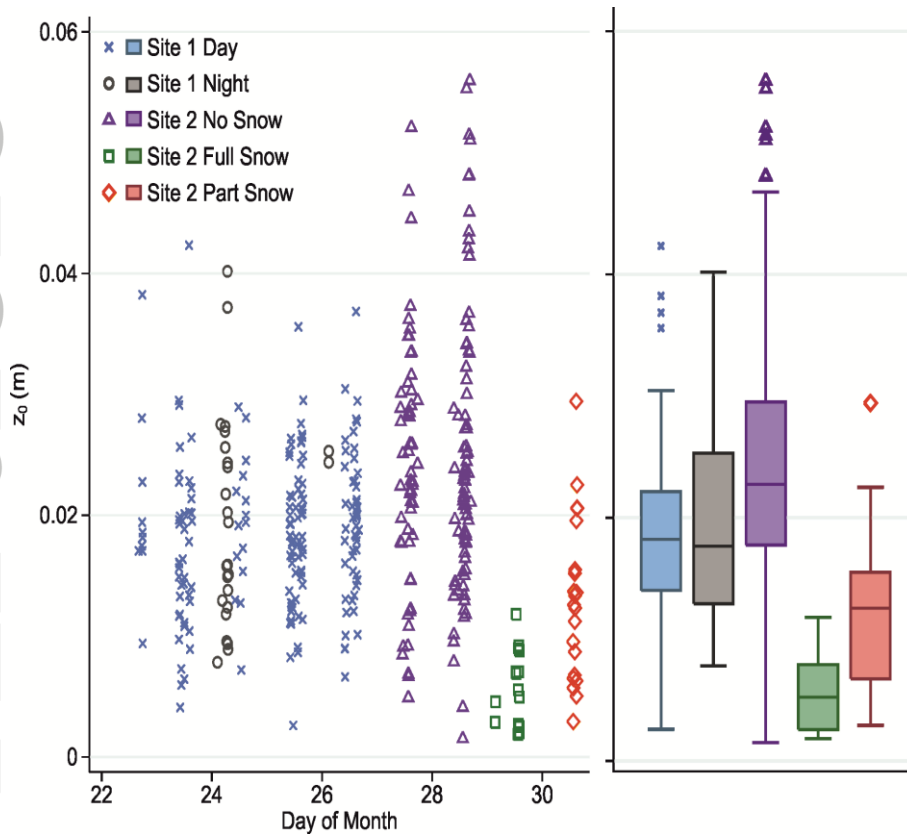


Figure 4: measurements of  $z_0$  derived from wind profile data at each site. Boxes show upper quartiles, medians and lower quartiles; whiskers extend to cover all points within 1.5 times the interquartile range of the quartiles; other points are shown separately.

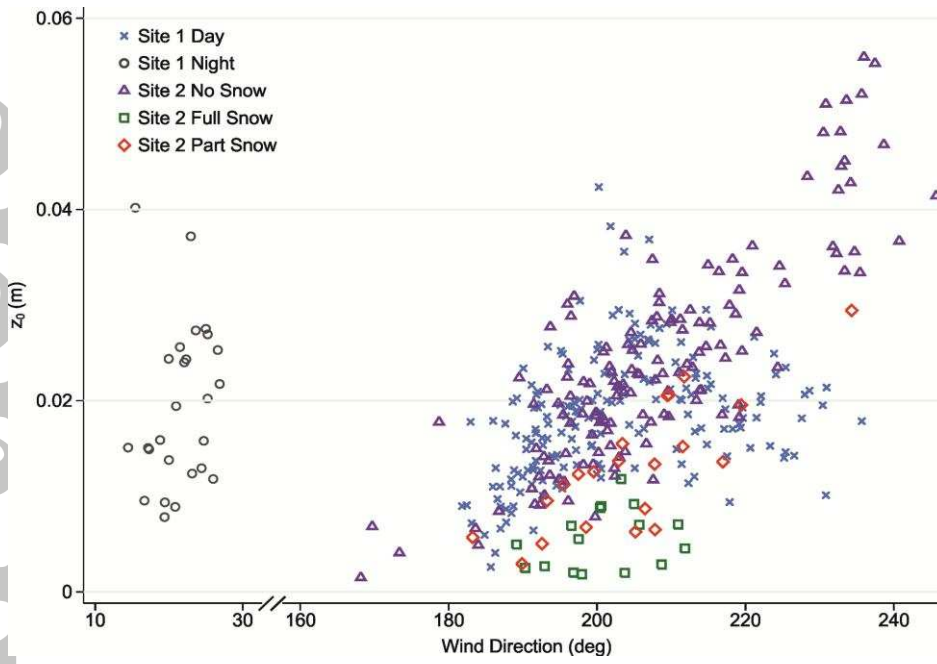


Figure 5: variations in  $z_0$  measurements with wind direction, derived from wind profile data at all sites.

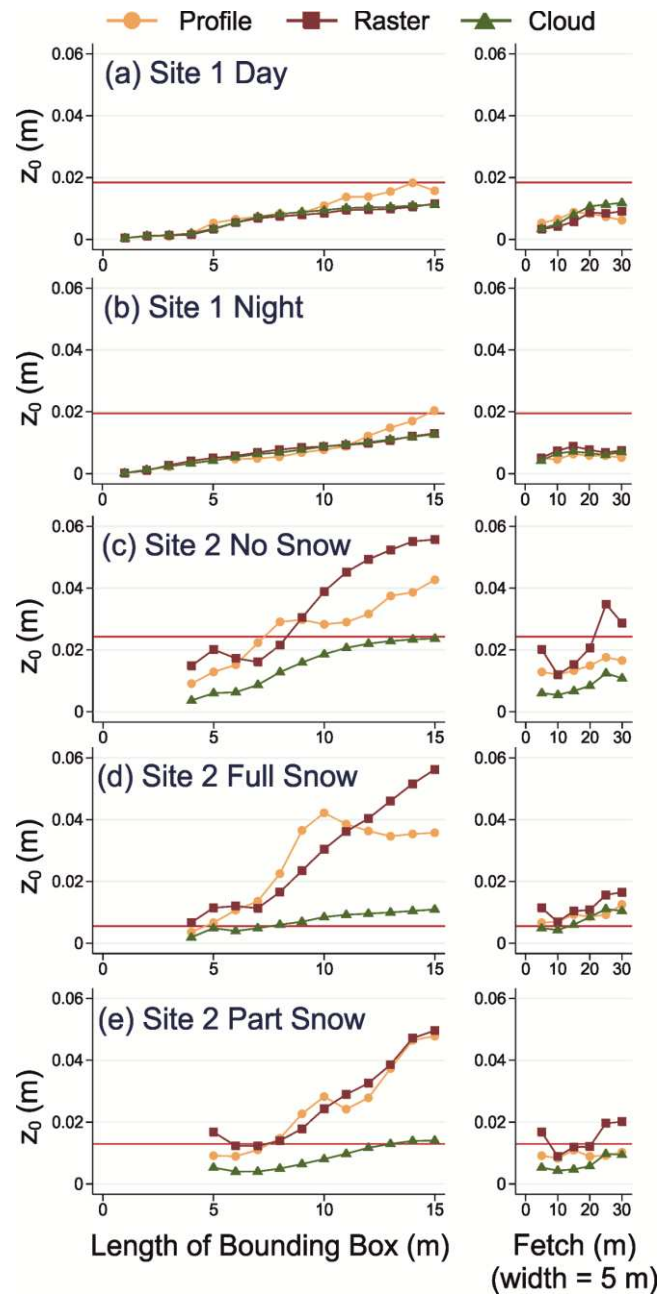


Figure 6: performance of the three methods at each site and varying patch width and length (left) and length only (right). Note values at smaller patch sizes are omitted where point cloud data were sparse, and the horizontal red line is measured mean  $z_0$ . Data used in the profile- and raster-based methods were 10 mm resolution.

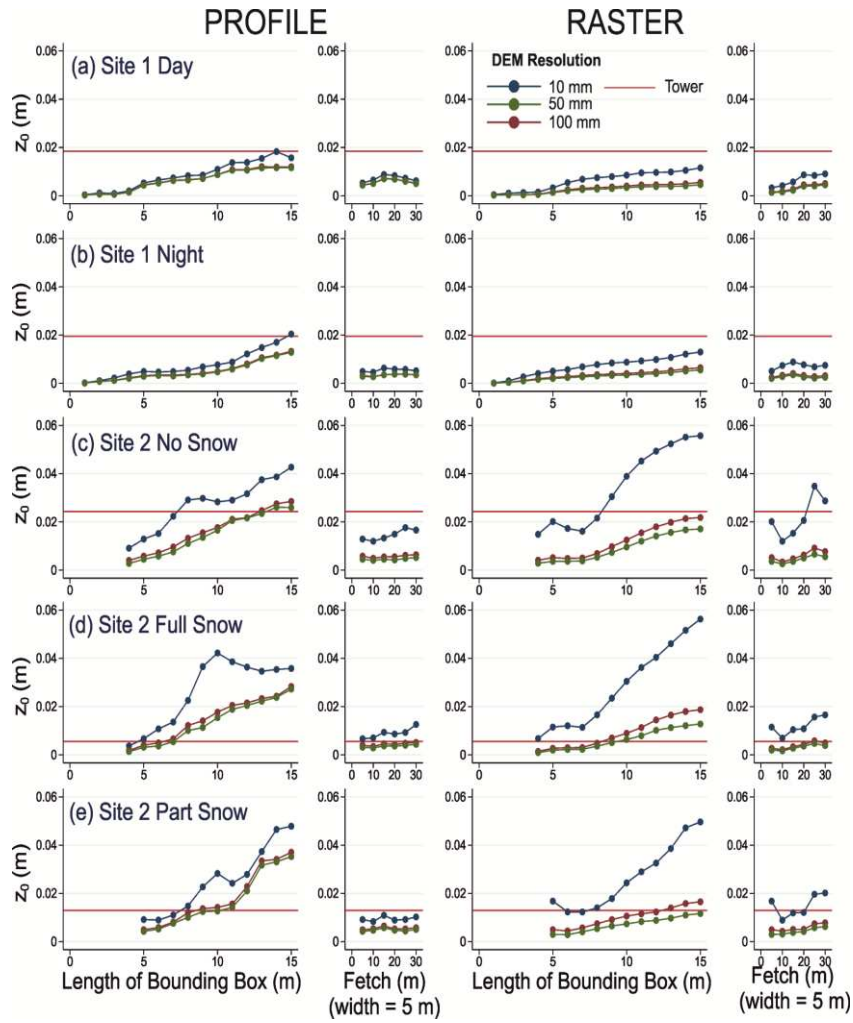


Figure 7: the effect of grid resolution on calculated  $z_0$  values varying by plot and by method. Note that red horizontal line is measured mean  $z_0$ .

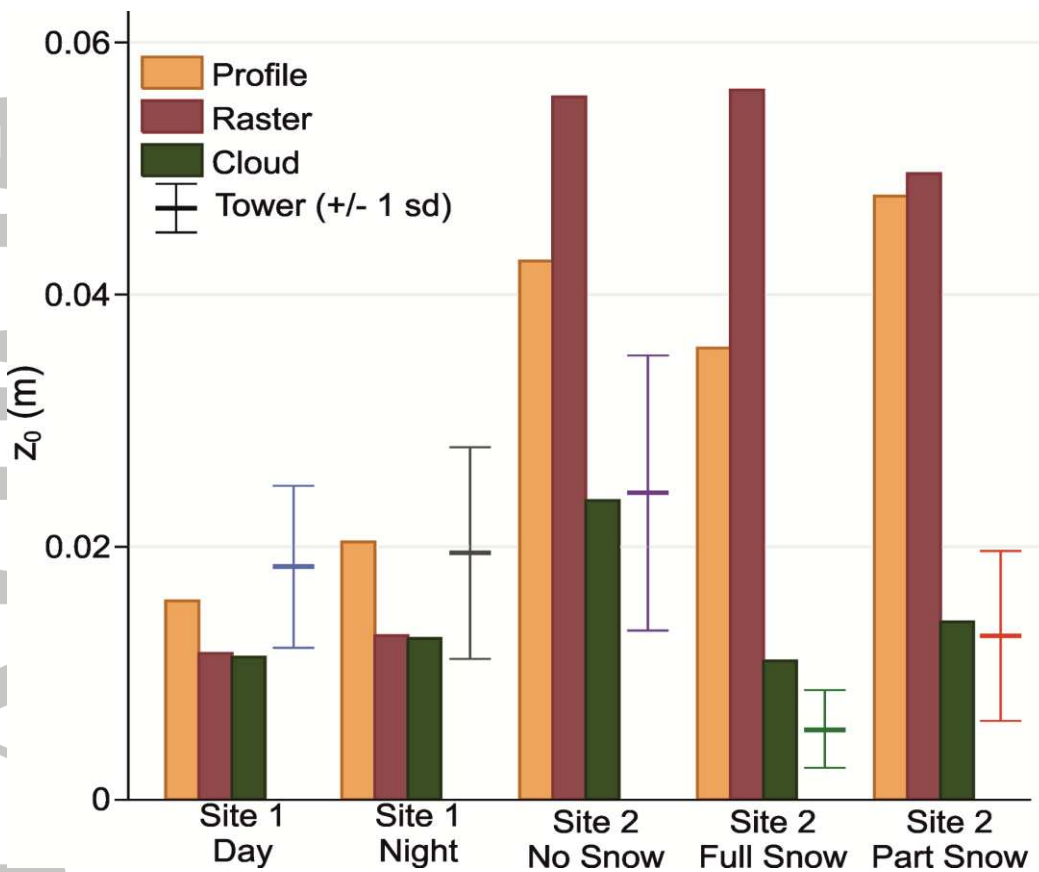


Figure 8: comparison of different methods against calculated wind tower values using 15 m x 15 m plots. Mean and  $\pm 1$  sd are shown for tower data.

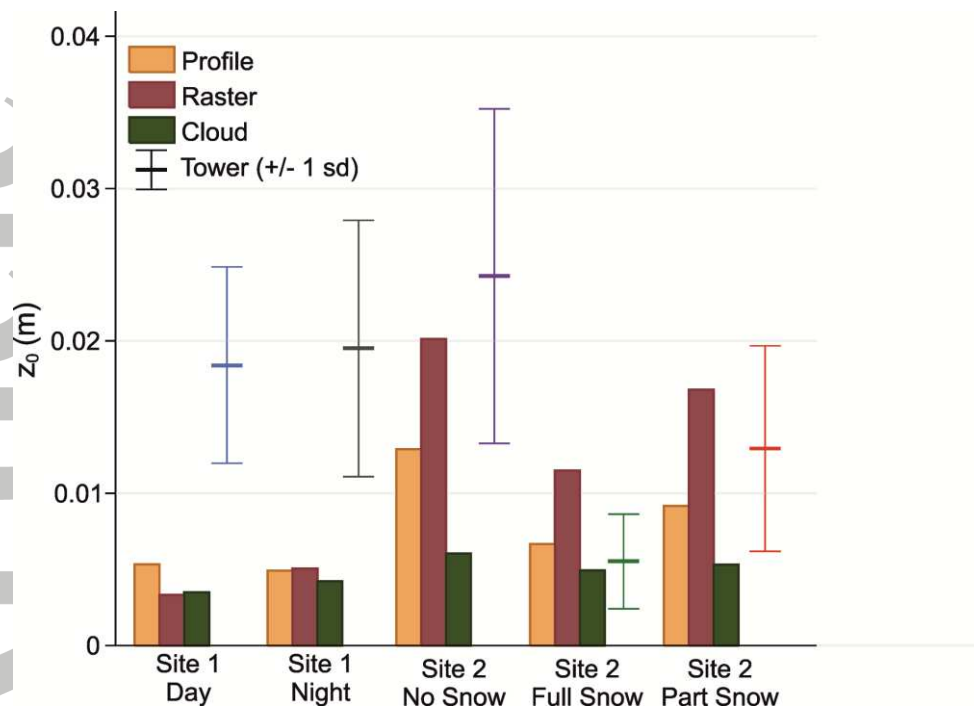


Figure 9: comparison of different methods against calculated wind tower values using 5 m x 5 m plots. Mean and  $\pm 1$  sd are shown for tower data.